

# Luminous and Variable Stars in M31 and M33. I. The Warm Hypergiants and Post-Red Supergiant Evolution<sup>1</sup>

Roberta M. Humphreys,<sup>2</sup> Kris Davidson,<sup>2</sup> Skyler Grammer,<sup>2</sup> Nathan Kneeland,<sup>2</sup> John C. Martin,<sup>3</sup> Kerstin Weis,<sup>4</sup> and Birgitta Burggraf,<sup>4</sup>

## ABSTRACT

The progenitors of Type IIP supernovae have an apparent upper limit to their initial masses of about  $20 M_{\odot}$ , suggesting that the most massive red supergiants evolve to warmer temperatures before their terminal explosion. But very few post-red supergiants are known. We have identified a small group of luminous stars in M31 and M33 that are candidates for post-red supergiant evolution. These stars have A – F-type supergiant absorption line spectra and strong hydrogen emission. Their spectra are also distinguished by the Ca II triplet and [Ca II] doublet in emission formed in a low density circumstellar environment. They all have significant near- and mid-infrared excess radiation due to free-free emission and thermal emission from dust. We estimate the amount of mass they have shed and discuss their wind parameters and mass loss rates which range from a few  $\times 10^{-6}$  to  $10^{-4} M_{\odot} \text{ yr}^{-1}$ . On an HR Diagram, these stars will overlap the region of the LBVs at maximum light, however the warm hypergiants are not LBVs. Their non-spherical winds are not optically thick and they have not

---

<sup>1</sup>Based on observations with the Multiple Mirror Telescope, a joint facility of the Smithsonian Institution and the University of Arizona and on observations obtained with the Large Binocular Telescope (LBT), an international collaboration among institutions in the United States, Italy and Germany. LBT Corporation partners are: The University of Arizona on behalf of the Arizona university system; Istituto Nazionale di Astrofisica, Italy; LBT Beteiligungsgesellschaft, Germany, representing the Max-Planck Society, the Astrophysical Institute Potsdam, and Heidelberg University; The Ohio State University, and The Research Corporation, on behalf of The University of Notre Dame, University of Minnesota and University of Virginia.

<sup>2</sup>Minnesota Institute for Astrophysics, 116 Church St SE, University of Minnesota, Minneapolis, MN 55455; roberta@umn.edu

<sup>3</sup>University of Illinois, Springfield, IL

<sup>4</sup>Astronomical Institute, Ruhr-Universitaet Bochum, Germany,

exhibited any significant variability. We suggest, however, that the warm hypergiants may be the progenitors of the “less luminous” LBVs such as R71 and even SN1987A.

*Subject headings:* galaxies:individual(M31,M33) – stars:massive – supergiants

## 1. Introduction

The progenitors of Type IIP supernovae have an apparent initial mass upper limit of about 20 solar masses (Smartt 2009), suggesting that red supergiants with higher initial masses do not explode as Type IIP SNe. Thus the most luminous red supergiants may evolve to warmer temperatures before their terminal explosions. This leaves us with the problem of where are these post-red supergiants and how do we recognize them? This is an important question for understanding the final stages of massive star evolution.

As part of a larger program on the luminous and variable stars in M31 and M33, we have identified a small subset of stars which we call warm hypergiants which may be post-red supergiants. In this first paper on the M31 and M33 stars, we describe the warm hypergiants and the evidence that they may be examples of post-red supergiants. In Paper II we will present the results of our spectroscopic survey of LBVs, candidate LBVs, emission line stars and other supergiants in M31 and M33, and in Paper III we will discuss the evidence for variability and instability in these stars.

In the next section we describe our new observations. Inspection of the spectra quickly revealed a few stars in each galaxy with A to F-type supergiant spectra and strong hydrogen emission. Their distinguishing characteristics, however, are the presence of the Ca II triplet near 8500Å and [Ca II] doublet near 7300Å in emission, indicating extensive circumstellar ejecta plus excess infrared radiation. The individual stars are described in §3, and in §4 we present the evidence for circumstellar nebulae, dusty ejecta, and significant mass loss in these stars. Their evolutionary state is discussed in the last section.

## 2. Target Selection and Spectroscopy

We selected known LBVs and LBV candidates, luminous emission-line stars, and evolved variables from the survey by Massey et al. (2007), an unpublished H $\alpha$  survey by Weis and collaborators, and the list of candidates from Valeev et al. (2010a). The observations were made in October 2010 with the Hectospec Multi-Object Spectrograph (MOS) (Fabricant et al

1998) on the 6.5-m MMT on Mt. Hopkins. The Hectospec<sup>1</sup> has a 1° FOV and uses 300 fibers each with a core diameter of 250 $\mu$ m subtending 1''.5 on the sky. Fibers were assigned to 27 stars in M31 and 57 in M33. We used the 600 l/mm grating with the 4800Å tilt yielding  $\approx$  2500Å coverage with 0.54Å/pixel resolution and R of  $\sim$  2000. The same grating with a tilt of 6800Å was used for the red spectra with  $\approx$  2500Å coverage, 0.54Å/pixel resolution and R of  $\sim$  3600. The blue and red spectra were reduced using an exportable version of the CfA/SAO SPECROAD package for Hectospec data<sup>2</sup>. The spectra were all bias subtracted, flatfielded and wavelength calibrated. Because of crowding, the sky subtraction was done using fibers assigned outside the field of the galaxy. For this reason, some of the spectra exhibit obvious nebular contamination. A journal of the observations is included in Table 1.

A few stars of special interest (5 in M31 and 8 in M33) were also observed with the MODS1 spectrograph on the Large Binocular Telescope (LBT) during commissioning in September 2011, and in October and November 2012, and January 2013. The MODS1 uses a dichroic to obtain blue and red spectra simultaneously with the G400L and G750L gratings for the blue and red channels, respectively, yielding wavelength coverage from 3200Å in the blue to more than 1 $\mu$ m in the red. With a 0''.6 slit the resolution is  $\sim$  2000. The two dimensional images were initially reduced by R. W. Pogge in 2011 following standard procedures for bias subtraction and flat fielding. The spectra from 2012 and 2013 were similarly reduced using software provided by R. W. Pogge for the MODS spectra. The spectra were then extracted and wavelength, and flux calibrated using the IRAF twodspec and onedspec packages. The observations of these individual stars are also listed in Table 1.

### 3. The Warm Hypergiants

The warm hypergiants are an especially interesting and significant class of objects for understanding the final stages and pre-SN evolution of massive stars. These stars, like IRC+10420 (Jones et al. 1993; Oudmaijer et al. 1996; Oudmaijer 1998; Humphreys et al. 1997; Humphreys, Davidson, & Smith 2002),  $\rho$  Cas (de Jager 1998; Lobel, et al. 2003; Gorlova et al. 2006), and HR8752 (Nieuwenhuijzen et al. 2012) in the Milky Way, are most likely on a post-red supergiant blue loop to warmer temperatures. The warm hypergiants in M31 and M33 include the peculiar Var A in M33 (Humphreys, Jones, & Gehrz 1987; Humphreys et al. 2006) and B324 in M33 (Humphreys 1980; Humphreys, Massey, & Freedman 1990; Massey et al.

---

<sup>1</sup><http://www.cfa.harvard.edu/mmti/hectospec.html>

<sup>2</sup>External SPECROAD was developed by Juan Cabanela for use on Linux or MacOS X systems outside of CfA. It is available online at: <http://iparrizar.mnstate.edu>.

1996; Clark et al. 2012), one of its visually brightest stars.

Based on their absorption lines, these stars have A to F-type supergiant spectra and strong hydrogen emission, hence the “warm” hypergiant name. The A – F spectrum may correspond to the star’s actual photosphere or it may originate in an optically thick wind, see §4. As discussed below several of these stars show spectroscopic evidence for winds and mass loss. In either case, the absorption-line spectrum represents the region from which the visual light is escaping. A critical characteristic of these stars is the presence of the near-infrared Ca II triplet in emission and the rare [Ca II]  $\lambda 7291$  and  $\lambda 7323$  emission lines. The [Ca II] doublet arises from the lower level of the transition that produces the triplet ( $\lambda\lambda 8498, 8542, 8662$ ) emission lines, which are formed in the star’s ejecta by radiative de-excitation from the strong Ca II H and K absorption upper levels. The [Ca II] levels are normally collisionally de-excited back to the ground state unless the density is sufficiently low. The [Ca II] emission lines thus imply a low density circumstellar medium. They are not commonly seen in the cool, dense winds of classical LBVs at maximum, possibly because Ca II has a low ionization potential and is suppressed in the presence of UV radiation which may be present in the environment from the hot underlying star. R71 in the LMC did develop [Ca II] emission during its current maximum (Gamen et al. 2012; Mehner et al. 2013), the first recorded for an LBV in eruption. R71, however, may be an example of a giant eruption LBV (Mehner et al. 2013).

Massey et al. (2007) called some of these warm hypergiants “hot LBV candidates” and in one case a “P Cyg LBV candidate”. The presence of Ca II H and K, other absorption lines common in A to F-type supergiants, the luminosity sensitive O I triplet at  $\lambda 7774\text{\AA}$  in A and F-type supergiants, and the Ca II and [Ca II] emission lines, however, indicate that they are evolved, cooler stars. The individual stars are discussed below with examples of their blue and red spectra.

Although *Variable A* in M33 was one of the original Hubble-Sandage variables (Hubble and Sandage 1953), it is not an LBV. It is one of the very luminous, unstable stars that define the empirical upper luminosity boundary in the HR Diagram, see Humphreys & Davidson (1994). It experienced a high mass loss episode that lasted about 45 years. Its photometric and spectroscopic variability has been described in some detail by Humphreys et al. (1987, 2006). Briefly, in 1951, when it was one of the visually brightest stars in M33, it rapidly *declined* by 3 mag. We now know that this was due to a shift in its energy distribution to lower temperatures and to the formation of dust. In 1985-86, Var A had the spectrum of an M supergiant and a large infrared excess at  $10\mu\text{m}$ . Its large spectral and photometric variations had occurred at nearly constant bolometric luminosity. Twenty years later, its spectrum had returned to a warmer F-type photosphere consistent with its properties at

maximum light 50 years earlier (Humphreys et al. 2006). Although its colors have likewise shifted bluer, Var A has remained faint, but see Table 3 for an update on the magnitudes. Comparison with our spectra from 2003-04 shows little change, though the hydrogen emission may have weakened slightly. Our current spectrum from September 2011 shows that it still has a late F-type spectrum and prominent emission lines of Ca II in the near-infrared, [Ca II], and relatively strong lines of K I. The importance of these lines was discussed in Humphreys et al. (2006). The higher signal-to-noise Hectospec and MODS1 spectra also permit a more accurate estimate of its apparent spectral type as F8.

*B324* in M33 has been classified as A5 Iae (Humphreys 1980; Humphreys, Massey, & Freedman 1990) and F0-F5 Ia (Monteverde et al. 1996). Absorption lines in its MODS1 blue and red spectra closely resemble the current spectrum of IRC +10420 (Oudmaijer 1998; Humphreys, Davidson, & Smith 2002). The Sr II  $\lambda 4078$  and  $\lambda 4215$  lines, and the strong Fe II, Ti II blends at  $\lambda\lambda 4172, 4178$  indicate very high luminosity. The relative strengths of the Ca II  $\lambda 4227$  and Fe II  $\lambda 4233$  lines and the N I absorption lines in the red indicate that B324 is later than an early A-type supergiant but not as cool as a late F-type. Based on these lines we recommend a spectral type of A8 - F0.  $H\beta$  is in emission but the higher Balmer lines are in absorption. Weak Fe II and Ti II emission lines also observed in IRC +10420 are present at  $\lambda > 5000\text{\AA}$ . The red spectrum shows strong  $H\alpha$  emission with broad wings, a strong O I triplet in absorption, plus the Ca II triplet and [Ca II] doublet in emission indicating the presence of low density circumstellar material. The Ca II triplet emission lines also have P Cygni absorption components. Several Fe II emission lines plus strong Si II absorption at  $\lambda 6347\text{\AA}$  and  $\lambda 6371\text{\AA}$  are also present between  $6000\text{\AA}$  and  $H\alpha$ .

Massey et al. (1996) and more recently Clark et al. (2012) have suggested on the basis of possible spectral variability that B324 may be an LBV candidate or an LBV in an extended maximum light, cool dense wind state, i.e. an LBV eruption. However, that conclusion is based on a limited apparent spectral type change (see above). Its current spectrum from a high quality digital spectrum is consistent with a very high luminosity late A-type supergiant. Furthermore the strong Ca II and [Ca II] emission and lack of variability cast doubt on whether it is an LBV. Instead B324 shares the spectral characteristics of IRC +10420 and other warm hypergiants. B324 also has a small near-infrared excess due to free-free emission in its wind (Figure 14). Clark et al. also argued that B324 was above the empirical upper luminosity boundary even though it was one of the stars that defined it (Humphreys 1983). Their conclusion however depended on a larger adopted distance modulus for M33 derived from an eclipsing binary (Bonanos et al. 2006) which was 0.6 mag higher than that used by Humphreys (1983). In this work we use the Cepheid distance scale, see §4.3. The luminosities of B324 and the other warm hypergiants are discussed there.

The MODS1 blue and red absorption line spectra of *N093351* and *N0125093* resemble those of B324 and IRC+10420. Both spectra show the critical Ca II triplet and [Ca II] emissions. The [Ca II] lines in N093351 however are very strong relative to the Ca II triplet which have asymmetric double emission profiles with a weaker blue component. The H $\alpha$  emission line is also double with a weaker blue component. Although the depths of the absorption minima in the Ca II lines and H $\alpha$  are not as deep as in IRC +10420, this is another characteristic it shares with IRC +10420 possibly due to a bipolar outflow. The velocities of the blue and red emission components relative to the absorption minima in the Ca II triplet lines indicate an outflow of about  $\pm 70$  km s $^{-1}$  and in H $\alpha$  the relative velocities are  $\pm 120$  km s $^{-1}$ . The [Ca II] emission lines are single and have velocities that agree with the absorption minima in the Ca II triplet profiles. The H $\alpha$  profile in N125093 also has an additional emission component on its blue side corresponding to an outflow velocity of  $\approx \pm 200$  km s $^{-1}$ . The H $\alpha$  and H $\beta$  line profiles in both stars have broad wings with a P Cygni absorption feature at H $\beta$ . Both stars also have an infrared excess due to circumstellar dust. N093351 and N0125093 have been proposed to be LBVs (Valeev et al. 2009, 2010b), but their spectral characteristics, infrared excess, and limited variability are more like IRC +10420 and B324.

The blue and red MODS1 spectra of B324, N093351, N0125093, and Var A are shown in Figure 1. N093351’s double H $\alpha$  and Ca II triplet profiles and the [Ca II] emission profiles are also shown separately in Figure 2. The H $\alpha$  and H $\beta$  profiles for the warm hypergiants are discussed in the next section on Thomson scattering (§4.2) and are shown in Figures 5 – 10 in the on-line edition.

We have also identified three warm hypergiants in M31 with the Ca II and [Ca II] emission. Massey et al. (2007) called *M31-004444.52* a P Cyg LBV candidate<sup>3</sup>. The Balmer and Fe II emission lines do indeed show deep P Cygni absorption features, but it is spectroscopically much more like IRC +10420 than P Cyg. M31-004444.52 not only has the signature Ca II and [Ca II] emission, but also strong O I  $\lambda 7774$  absorption, and Ca II H and K and other absorption lines characteristic of luminous A and F-type supergiants such as the Fe II, Ti II blends at 4172Å and 4178Å. Based on its absorption lines its apparent spectral type is  $\approx$  F0. The hydrogen emission profiles are asymmetric and concave to the red with very broad wings, the characteristic signature of Thomson scattering very likely in the star’s wind (§4.2 and Figure 4), plus deep P Cygni absorption. The strong Fe II emission lines from multiplet 42 ( $\lambda\lambda 4924, 5018, 5169$ ) display the same asymmetric profiles from Thomson scattering with P Cyg features. The Ca II and [Ca II] emission profiles are similarly asymmetric and the Ca

---

<sup>3</sup>In this paper we use the galaxy name plus the RA of the star as its designator.

II triplet lines also show P Cyg absorption.

The spectrum of *M31-004522.58* shows the higher Balmer lines in absorption, the Ca II K line, He I 4026Å and 4009Å in absorption together with weak Fe II emission. These He I lines plus the relative strengths of the He I  $\lambda$ 4471Å and Mg II  $\lambda$ 4481Å absorption lines suggest a somewhat earlier spectral type than for the other hypergiants,  $\approx$  A2.  $H\alpha$  also has a double emission line profile with broad wings resembling N093351 in M33. The relative velocities of the blue and red emission components are  $\approx \pm 105$  km s $^{-1}$  with respect to the absorption minimum. The Ca II triplet lines, however, are not double, although a higher resolution spectrum might show similarly double profiles. In addition to Ca II and [CaII], O I 8446Å is in emission. The O I blend at 7774Å is very weakly present in absorption. We would normally expect to see both O I lines in emission in about equal strength, but 8446Å can be pumped by fluorescence with Lyman  $\beta$ . Thus O I 7774Å is probably at least partially filled in by emission.

Although the blue and red Hectospec spectra of *M31-004322.50* have low S/N, there are numerous absorption lines in the blue characteristic of late A or early F-type supergiants, a strong O I 7774Å line in absorption and the [Ca II] doublet in emission. Its spectrum is very much like that of M31-004444.52.  $H\alpha$  and  $H\beta$  have asymmetric profiles with broad red wings characteristic of Thomson scattering and deep P Cygni absorption features. This asymmetry is shared with the three strong Fe II emission lines at 4924Å, 5018Å, and 5169Å from multiplet 42 also with P Cygni absorption. The Hectospec red spectra do not go past 8000Å, so we cannot confirm if the Ca II triplet is in emission. The blue and red spectra of the three warm hypergiants in M31 are shown in Figure 3, and their  $H\alpha$  and  $H\beta$  emission profiles are shown in Figure 4 for M31-004444.52 and in Figures 5 – 10, in the on-line edition.

The warm hypergiants are listed in Table 2 with their positions and apparent spectral types. Only one of these stars, N125093 in M33, is the lists of candidate yellow supergiants by Drout et al. (2009, 2012). The visual photometry from Massey et al. (2006) and near- and mid-infrared photometry from cross-identification with 2MASS (Cutri et al 2003), the *Spitzer* surveys of M31 (Mould et al. 2008) and M33 (McQuinn et al. 2007; Thompson et al. 2009) and WISE (Wright et al. 2010) is summarized in Table 3. All of the warm hypergiants have excess infrared emission. Their resulting spectral energy distributions (SEDs), circumstellar ejecta, and mass loss indicators are discussed in the next section.

## 4. Circumstellar Nebulae, Winds, Dusty Ejecta, and Mass Loss

### 4.1. The Gaseous Circumstellar Ejecta

The spectra of the warm hypergiants display a variety of indicators for extensive circumstellar gas, stellar winds, and mass loss. These include deep P Cygni absorption profiles, Thomson scattering wings formed in their stellar winds, and the Ca II, [Ca II] emission lines. Three of these stars show double emission profiles in H $\alpha$ , and in Ca II in one star, probably due to bipolar outflows. The outflow velocities measured from the double profiles and the absorption minima in the P Cygni profiles are summarized in Table 4. The velocities range from less than 100 km s<sup>-1</sup> up to  $\sim 300$  km s<sup>-1</sup> and are typical for A to F-type supergiants. We note that there is tendency for the velocities from the Ca II and [Ca II] emission lines to be somewhat lower than those for the hydrogen and Fe II lines in the same star. The Ca II and [Ca II] lines may be formed in a different region than the other lines which can originate in denser gas closer to the star.

We estimate the densities in the outflow from the ratio of the [Ca II]  $\lambda 7300$  and Ca II triplet circa  $\lambda 8500$  equivalent widths of the emission multiplets. The Ca II triplet emission is produced by radiative de-excitation from the absorption from the strong Ca II H and K lines ( $4s\ ^2S \rightarrow 4p\ ^2P^o$ ) in the star’s photosphere. The transition  $4p\ ^2P^o \rightarrow 3d\ ^2D$  that produces the Ca II triplet emission leaves the atoms in the upper levels for the forbidden lines. Collisional excitation is much weaker at the relevant temperatures and densities. However, some of the  $3d \rightarrow 4s$  photons are eliminated by collisional de-excitation, whose critical electron density is  $n_c \approx 8 \times 10^6$  cm<sup>-3</sup> at temperatures around 8000 K. Therefore the ratio of photon fluxes in the two multiplets should be approximately

$$\frac{\Phi(\lambda 7300)}{\Phi(\lambda 8600)} \approx \left(1 + \frac{n_e}{n_c}\right)^{-1}, \quad (1)$$

where  $n_e$  is a suitable average electron density in the emission region. For this calculation we used radiative transition and collision strengths for Ca II from Melendez, Bautista & Badnell (2007). The photon ratios and corresponding electron densities are given in Table 5 for the six hypergiants with Ca II triplet data. The densities range from  $\sim 1$  to  $4 \times 10^7$  cm<sup>-3</sup> and are comparable to our previous results for IRC +10420 (Jones et al. 1993; Humphreys, Davidson, & Smith 2002) with  $n_e$  of  $2.5 \times 10^7$  cm<sup>-3</sup>. With reasonable mass loss rates, such densities should occur at  $r \sim 30$  stellar radii.

The above reasoning is subject to an obvious proviso, however. One can easily imagine a two-component model, wherein a denser region emits permitted Ca II emission but very little forbidden emission, while a physically distinct low-density region accounts for nearly all of the [Ca II] but only a fraction of the Ca II triplet. In that case the derived  $n_e$  must

be re-interpreted; instead of a weighted average density,  $n_e$  becomes a lower limit for one component and an upper limit for the other. In some of these objects a two-component model is supported by differences between the permitted and forbidden line profiles (Fig. 2). This type of model is very consistent with suspicions that the wind is strongly non-spherical, see below.

## 4.2. Thomson Scattering and Mass Loss

The hydrogen emission profiles in the warm hypergiants exhibit broad Thomson scattering wings, and in some cases the characteristic asymmetric profiles are also observed in other emission lines such as the Ca II triplet and the strong Fe II emission lines. The Thomson-scattered wings can help constrain the wind parameters and mass loss. The two best examples in this paper are M31-004444.52 and M31-004322.50 which have asymmetric electron scattering profiles present in both the hydrogen and Fe II emission lines, see Figures 3 and 4. On the red side of H $\alpha$  and H $\beta$  in M31-004444.52, for instance, one can see a line wing at velocities of 800 km s $^{-1}$  or more from the line peak (Figure 4), though the line core has a FWHM of only 200 km s $^{-1}$ , and the P Cyg absorption implies a terminal velocity not much above 300 km s $^{-1}$ . Thus the overall shape and physical context are consistent with Thomson scattering. The H $\alpha$  and H $\beta$  emission profiles for the other hypergiants are shown in Figures 5 – 10 in the on-line edition and their H $\alpha$  equivalent widths are included in Table 6. (Examples of line profiles with stronger Thomson-scattered wings are shown in Fig. 11 in Dessart et al. 2008, Fig. 8 in Humphreys et al. 2012 and several examples in hydrogen and Ca II in Humphreys et al. 2011.) A detailed model would be far beyond the scope of this paper, but here we briefly review the case.

Thomson-scattered line wings provide information about circumstellar densities and size scales. For these stars, however, the main implications are different because spherical models lead to interesting contradictions outlined below.

To illustrate the problem, consider a spherical model with idealized assumptions: (1) the outflow density is  $\rho(r) \propto r^{-2}$ , mostly ionized; (2) emission line photons emitted outside radius  $r_1$  escape, while those inside  $r < r_1$  are destroyed by continuum absorption or by conversion to other emission lines; (3) the line emissivity is  $A_l n_e^2$  where  $A_l$  is a known constant for each line; and (4)  $\tau_1$ , the Thomson scattering optical depth at radius  $r_1$ , is roughly indicated by the observed strength of the line wings. When this type of model is used for other, more luminous objects, its main results agree with more elaborate calculations within factors of two or three (e.g., compare Humphreys et al. 2012; Dessart et al. 2008; Davidson et al. 1995; Hillier et al. 2001). It is easy to show that the above assumptions

imply

$$r_1 \approx \frac{\sigma_e^2 L_l}{4 \pi A_l \tau_1^2}, \quad (2)$$

where  $\sigma_e$  is the Thomson scattering cross section and  $L_l$  is the emergent luminosity of the emission line. We apply this formula to H $\beta$  in M31-004444.52, for example. For a measure of the line wing, we estimate a flux ratio

$$\frac{F(300 \text{ to } 500 \text{ km s}^{-1})}{F(0 \text{ to } 500 \text{ km s}^{-1})} \approx 0.1,$$

where the velocities are measured relative to the line peak. Numerical simulations indicate that a scattering thickness  $\tau_1 \sim 0.8$  would account for this value. With reasonable values  $L_l \approx 4 \times 10^{36} \text{ erg s}^{-1}$  and  $A_l \approx 10^{-25} \text{ erg cm}^3 \text{ s}^{-1}$  (Osterbrock and Ferland 2006), eq. 1 then gives  $r_1 \approx 30 R_\odot$ . But this is absurd, because it is much smaller than the star’s radius  $R \sim 300 R_\odot$ . If we try to improve the model by allowing for local inhomogeneities in  $\rho$  (“clumping”), a radial dependence  $\rho(r)$  consistent with accelerating velocities, or a maximum radius for the ionization, then the deduced  $r_1$  becomes even smaller. The same discrepancy occurs for the other stars in our sample;  $\tau_1$  seems generally too large for the observed emission line fluxes.

If this contradiction were only a factor of two or three, then we could ascribe it to uncertainties in the parameters; but a discrepancy factor of 10 or more suggests that the line emission region is basically different from the above model. Here we consider three possibilities:

1. Conceivably the line wings are not due to Thomson scattering, and the true value of  $\tau_1$  is much less than 0.8. If so, however, then unexplained high velocities must be present, much faster than the stars’ escape velocities and the limits of the observed P Cyg features. In order to produce the observed fluxes in the wings, these high-velocity flows would need to carry a substantial fraction of the total mass loss rate. Moreover, they would most likely be non-spherical since we do not see high-velocity P Cyg absorption. (Radiative acceleration via dust is not useful for this hypothesis, because most of the line emission must be created much closer to the star than the dust-formation radius.)
2. Perhaps we have greatly overestimated the effective emissivity  $A_l$ , because most of the line photons may be absorbed before they escape. But this hypothesis is not as simple as it may appear. Semi-realistic models tend to have outer regions where escape is easy for a freshly created line photon, plus inner zones where most line photons are destroyed before they can escape. The *effective* rate  $A_l$  is only slightly reduced in the

outer zones but is almost nullified in the inner zones. In that case eq. 1 approximates the outer region, with  $r_1$  marking the ill-defined transition between the two regimes. Since  $A_l$  thereby represents mainly the region where most line photons escape, a factor-of-two alteration in its effective value may be unsurprising but a factor of 10 seems unlikely. Exact evaluations would depend on the definition of  $\tau_1$ , which is too complex to discuss here.

3. Eq. 1 becomes invalid in a non-spherical model. For instance, if only part of the spherical shell exists, then the factor  $4\pi$  in the denominator is reduced so  $r_1$  becomes larger. A bipolar flow may be able to achieve this result, and various other clues throughout this paper also suggest geometries of this type.

The second and third of these possibilities allow “reasonable” mass loss rates. For instance, consider again H $\beta$  in the case of M31-004444.52. Suppose that  $r_1 \sim R = 300 R_\odot$  with outflows covering about 15% of the solid angle,  $10^{-25.3} < A_l < 10^{-25.0}$  erg cm<sup>3</sup> s<sup>-1</sup>,  $\tau_1 \sim 0.8$ , and  $V_\infty \approx 300$  km s<sup>-1</sup>. We also make allowances for the effect of wind acceleration on  $\rho(r)$ . Then the observed H $\beta$  luminosity is consistent with  $\dot{M}/\epsilon$  in the range  $10^{-5}$  to  $10^{-4} M_\odot$  y<sup>-1</sup> where  $\epsilon$  is a standard volume-filling factor to allow for local inhomogeneities,  $0 < \epsilon < 1$ . (A mass loss range is estimated for M31-004444.52 and M31-004322.50 in Table 6 if  $\epsilon$  is  $\sim 1$ .) A more detailed discussion would be very lengthy and is beyond the scope of this paper, but the main point is this: the main parameters are reasonable *if we do not assume spherical symmetry*.

Bipolar outflows can explain why some of these objects show strong P Cyg absorption while others do not; why some but not all of them have asymmetric line profiles; and why double line peaks occur in some cases. The forbidden [Ca II] emission noted in §4.1 may originate in lower-density low-latitude zones of the outflow. Thus, although we cannot *prove* that these objects have polar outflows, the concept is very appealing.

The line profiles also imply that the winds are not opaque in the continuum; in other words the photospheres do represent stellar surfaces and not dense outflows. Based on “thermalization depth” arguments, the color-temperature photosphere in an opaque wind usually corresponds to a Thomson-scattering optical depth of the order of 3 (Davidson 1987). Therefore an opaque wind should be accompanied by Thomson-scattered emission line wings with  $\tau_1 \sim 2$ , appreciably larger than the  $\tau_1 < 1$  estimated above.

### 4.3. Circumstellar Dust and Mass Loss

The SEDs of almost all of the stars described here show the presence of circumstellar dust in addition to the gaseous ejecta. The SEDs are shown in Figures 11 and 12 for the M31 and M33 stars, respectively. Var A is shown separately in Figure 13 reproduced from (Humphreys et al. 2006) with the more recent photometry from WISE and its current V magnitude (Table 3). The one exception is B324 shown in Figure 14. Its interstellar extinction corrected SED instead shows significant near-infrared radiation due to strong free-free emission from its wind. We attribute its apparent excess longwards of  $10\mu\text{m}$  from the WISE data to PAH and dust emission from an H II region. B324 is in a dense association (No. 67 in Humphreys & Sandage 1980) of luminous, young stars and their associated nebulosity. The  $\text{H}\alpha$  image from Massey et al. (2006) shows B324 embedded in emission nebulosity.

The SEDs of the remaining warm hypergiants show thermal emission from dust to varying degrees in the near- and mid-infrared from  $3.5\mu\text{m}$  to  $8\mu\text{m}$  in the IRAC data and in most cases the WISE data shows that the thermal emission also extends to even longer wavelengths. We can use the flux at mid-infrared wavelengths to estimate the mass of the dusty circumstellar material with some assumptions about the grains.

The dust mass is given by

$$M_{dust} = \frac{4D^2\rho\lambda F_\lambda}{3(\lambda Q_\lambda/a)B_\lambda(T)},$$

where  $D$  is the distance to M31 or M33,  $F_\lambda$  is the mid-infrared flux,  $a$  is the grain radius,  $\rho \approx 3 \text{ g cm}^{-3}$  is the grain density,  $Q_\lambda$  is the grain efficiency for the absorption and emission of radiation, and  $B_\lambda(T)$  is the Planck specific intensity at temperature  $T$ .

The SEDs of the warm hypergiants are relatively flat suggesting that the dust grains are radiating at a range of temperatures from possibly as warm as 1000 K to 300 K at  $10\mu\text{m}$  and in an extended zone from  $\sim 100 \text{ AU}$  to several 100 AU from the star. Except for Var A, we do not have a measurement of the  $9.8$  and  $18\mu\text{m}$  silicate features. We therefore adopt the flux at  $8\mu\text{m}$  for the other stars and an assumed grain temperature of 350 K for this calculation using the formulation from Suh (1999) for  $Q_\lambda$  with  $a = 0.1\mu\text{m}$ . Assuming the nominal gas to dust ratio of 100 we then derive estimates of the total mass lost in Table 6. The results show a range of at least a factor of 10 for the mass of the circumstellar material, although most of the hypergiants have apparently shed about  $2 \times 10^{-2} M_\odot$ .

For Var A, we use the flux in the  $9.8\mu\text{m}$  silicate feature to estimate the mass loss and its mass loss rate at two different times, during its high mass loss event (1986) and after its cessation had begun (2004), see Figure 7. Not surprisingly these give different mass loss

estimates. Assuming that the dust formed as a result of the high mass loss event in 1951, we find a mass loss rate during the event of  $5 \times 10^{-4} M_{\odot} \text{ yr}^{-1}$  which declined to an average of  $1.5 \times 10^{-4} M_{\odot} \text{ yr}^{-1}$  after Var A had transitioned back to its warmer state. The former value agrees with our earlier result (Humphreys, Jones, & Gehrz 1987) using an independent method.

We also determine the total or bolometric luminosities of the hypergiants by integrating their SEDs from  $0.35\mu\text{m}$  to  $10\mu\text{m}$ , first corrected for interstellar extinction. There is always some uncertainty associated with visual extinction estimates from the observed colors for stars with emission lines in their spectra. We therefore estimate the extinction the classical way from the observed  $B - V$  color and apparent spectral type, and also for comparison, from nearby stars assuming that their UBV colors from Massey et al. (2006) are normal. We adopt  $R = 3.2$  mag for the ratio of total to selective extinction. For example, the observed  $B - V$  colors for N093351 would imply essentially zero reddening for its apparent spectral type even though the foreground  $A_v$  for M33 is  $\approx 0.3$  mag. Two nearby stars, including UIT231 (Massey et al. 1996) plus a fainter OB star, give  $A_v$  of 0.5 and 0.4 mag. We therefore adopt 0.45 mag for N093351. A similar situation occurs for M31-004522.58. For three of the other stars, however the extinction estimate from the colors was systematically higher than from the neighboring stars (Table 7). The only star for which the two  $A_v$  estimates are comparable, B324, has little or no circumstellar dust, thus the higher  $A_v$  for the other stars from their colors might be due to additional circumstellar reddening. The higher extinction values also produced SEDs in the visual more consistent with the temperatures expected from their spectra. We therefore adopted  $A_v$  from the observed colors. For purposes of comparing stars in different galaxies we use the Cepheid distance scale with moduli, 24.4 mag for M31 (Riess et al. 2012) and 24.5 mag for M33 (Scowcroft et al. 2009) for the luminosities in Table 7.

B324 is the most luminous with an absolute bolometric magnitude of -10.1 and a luminosity of  $\approx 8 \times 10^5 L_{\odot}$  using this distance for M33 and the visual magnitudes measured from the HST images (Table 3). At a temperature of  $\sim 8000$  K, it is not above the empirical upper luminosity boundary. Instead, as one of the visually most luminous stars in M33, B324 is one of the stars that defines it for that galaxy.

Var A's luminosity in Table 7 may appear anomalously low. Based on its visual maximum in 1951 and its infrared flux in 1986 (Humphreys, Jones, & Gehrz 1987), its absolute bolometric magnitude was  $\approx -9.5$  ( $5 \times 10^5 L_{\odot}$ ). We (Humphreys et al. 2006) showed that after about 45 yrs, Var A's high mass loss event had ceased. Its spectrum and colors had returned to its F supergiant state, although it remained obscured, and the  $10\mu\text{m}$  flux and corresponding mass loss rate (see above) had declined. As we emphasized in 2006, a decrease

in total luminosity by a factor of 3 – 5 is unrealistic. Consequently we concluded that much of the radiation must be escaping from out of our line of sight. With the recent evidence that Var A may be starting to brighten in the visual, continued observations may provide clues to the structure of its circumstellar ejecta and mass loss as it recovers from its high mass loss episode.

Except for M31-004322.50, which is significantly fainter than the other stars, the warm hypergiants have luminosities that suggest they had initial masses above  $20 M_{\odot}$  with some of them likely above  $30 M_{\odot}$ .

## 5. Comments on the Evolutionary State of the Warm Hypergiants

It has been acknowledged for some time that the Galactic hypergiant IRC +10420 is a post-red supergiant (Jones et al. 1993; Oudmaijer et al. 1996). Var A and  $\rho$  Cas (de Jager 1998), with their apparent transits in the HR Diagram, are likely in a similar unstable post-RSG state. In this paper we are suggesting that these seven stars in M31 and M33, including Var A, are candidates for post-red supergiant evolution. They have the characteristics we would expect; A to F-type absorption spectra, winds with relatively slow outflows, an extensive and dusty circumstellar ejecta, and relatively high mass loss. B324 may be the one exception. Although it has a low density circumstellar envelope, it lacks a dusty environment, but then so do  $\rho$  Cas and HR 8752. Its evolutionary state is thus uncertain. It could just as easily be evolving towards cooler temperatures with significant mass loss due to its high luminosity or be on a blue loop as a post-RSG.

Some authors have previously suggested that some of these stars are LBVs, presumably in their maximum light phase when their optically thick winds resemble A to F-type supergiants. If these stars were above the empirical luminosity boundary in the HR Diagram, then it would be easy to argue that they are LBVs in their “eruption” state. But the warm hypergiants have luminosities that place them below the upper luminosity boundary. On the HR Diagram these warm hypergiants will lie between  $\approx 7000$  and  $9000\text{K}$  which does indeed overlap the maximum light phase for the LBVs (Figure 9 in Humphreys & Davidson (1994)). However unlike the LBVs, the winds of these warm hypergiants are not optically thick based on the discussion in §4.2.

Furthermore, the lack of significant variability over several decades for the M33 stars (Paper III) and no evidence of large brightness variation in the three M31 candidates, support a post-RSG origin as opposed to LBVs in an extended maximum. The warm hypergiants do show the small oscillations ( $\pm 0.1 - 0.2$  mag) typical of A to F-type supergiants, often referred

to as  $\alpha$  Cygni variability (see van Genderen & Sterken (2002) and references therein). LBVs at maximum light also exhibit  $\alpha$  Cygni variability, but during an extended maximum show larger variations of  $\pm 0.5$  mag or more (van Genderen et al. 1997a,b). The warm hypergiants, however, are very likely the progenitors of the “less luminous” LBVs which have presumably been red supergiants (Humphreys & Davidson 1994). They could indeed be the progenitors of a star like R71 or even SN 1987A.

We conclude by emphasizing that this is by no means a comprehensive survey for post-RSGs. These stars were identified as part of a larger program on the luminous and variable stars in M31 and M33 (Paper II). It is also possible that not all post-RSGs will share all of the characteristics of this small subset. Furthermore, as they evolve to warmer temperatures on their blue loops they may become harder to distinguish from the normal supergiants unless they do become LBVs or develop distinctive emission-line spectra perhaps like the Fe II emission-line stars with large infrared excesses discussed in our next paper.

Research by R. Humphreys and K. Davidson on massive stars is supported by the National Science Foundation grant AST-1019394. J.C. Martin’s collaborative work on luminous variables is supported by the National Science Foundation grant AST-1108890. This paper uses data from the MODS1 spectrograph built with funding from NSF grant AST-9987045 and the NSF Telescope System Instrumentation Program (TSIP), with additional funds from the Ohio Board of Regents and the Ohio State University Office of Research. This publication also makes use of data products from the Wide-field Infrared Survey Explorer, which is a joint project of the University of California, Los Angeles, and the Jet Propulsion Laboratory/California Institute of Technology, funded by the National Aeronautics and Space Administration.

*Facilities:* MMT/Hectospec, LBT/MODS1

## REFERENCES

- Bonanos, A. Z. et al. 2006, ApJ, 652, 313
- Clark, J. S., Castro, N., Garcia, M., et al. 2012, A&A, 541, A146
- Cutri, R. M., Skrutskie, M. F., Van Dyk, S. et al. 2003, The IRSA 2MASS All-Sky Point Source Catalog, NASA/IPAC Infrared Science Archive
- Davidson, K., Ebbets, D., Weigelt, G., Humphreys, R M., Hajian, A. R., Walborn, N. R., & Rosa, M. 1995, AJ, 109, 1784

- Davidson, K. 1987, *ApJ*, 317, 760
- de Jager, C. 1998, *A&A Rev.*, 8, 145
- Dessart, L., Hillier, D. J., Gezari, S., Ba sa, S. & Matheson, T. 2009, *MNRAS*, 394, 21
- Drout, M. R., Massey, P., Meynet, G., Tokarz, S., & Caldwell, N. 2009, *ApJ*, 703, 441
- Drout, M. R., Massey, P. & Meynet, G. 2012, *ApJ*, 750, 97
- Fabricant, D. G., Hertz, E. N., Szentgyorgyi, A. H., et al. 1998, *Proc. SPIE*, 3355, 285
- Gamen, R., Walborn, N., Morrell, N., Barba, R. & Fernandez-Lajus, E. 2012, *CBET* 3192
- Gorlova, N., Lobel, A., Burgasser, A. J., Rieke, G. H., Ilyin, I., & Stauffer, J. R. 2006, *ApJ*, 651, 1130
- Hillier, D. J., Davidson, K., Ishibashi, K., & Gull, T. R. 2001, *ApJ*, 553, 837
- Hubble, E. & Sandage, A. 1953, *ApJ*, 118, 353
- Humphreys, R. M. 1980, *ApJ*, 241, 587
- Humphreys, R. M & Sandage, A. 1980, *ApJS*, 44, 319
- Humphreys, R. M. 1983, *ApJ*, 269, 335
- Humphreys, R. M., Jones, T. J. & Gehrz, R. D. 1987, *AJ*, 94, 315
- Humphreys, R. M., Massey, P. & Freedman, W. L. 1990, *AJ*, 99, 84
- Humphreys, R. M. and Davidson, K. 1994, *PASP*, 106, 1025
- Humphreys, R. M., Smith, N., Davidson, K., et al. 1997, *AJ*, 114, 2778
- Humphreys, R. M., Davidson, K, & Smith, N. 2002, *ApJ*, 124, 1026
- Humphreys, R. M., Jones, T. J., Polomski, E., et al. 2006, *ApJ*, 131, 2105
- Humphreys, R. M., et al. 2011, *ApJ*, 743, 118
- Humphreys, R. M., Davidson, K., Jones, T. J., Pogge, R. W., Grammer, S. H., Prieto, J. L., & Pritchard, T. A. 2012, *ApJ*, 760, 93
- Jones, T. J., Humphreys, R. M., Gehrz, R. D. et al. 1993, *ApJ*, 411, 323
- Lobel, A., et al. 2003, *ApJ*, 583, 923

- Massey, P., Bianchi, L., Hutchings, J. B., & Stecher, T. P. 1996, ApJ, 469, 629
- Massey, P. & Johnson, O. 1998 ApJ, 505, 793
- Massey, P., Olsen, K. A. G., Hodge, P. W. et al. 2006, AJ, 131, 2478
- Massey, P., McNeill, R. T., Olsen, K. A. G., et al. 2007, AJ, 134, 2474
- McQuinn, K. B. W., Woodward, C. E., Willner, S. P. et al. 2007, ApJ, 664, 850
- Mehner, A., Baade, D, Rivinius, T., Lennon, D. J., Martayan, C., Stahl, O. & Steffi, S. 2013, A&A, submitted
- Melendez, M., Bautista, M. A., & Badnell, N. R. 2007, A&A, 469, 1203
- Monteverde, M. L., Herrero, A., Lennon, D. J. et al. 1996, A&A, 312, 24
- Mould, J., Barmby, P., Gordon, K., et al. 2008, ApJ, 687, 230
- Nieuwenhuijzen, H., De Jager, C., Kolka, I., Israelian, G., Lobel, A., Zsoldos, E., Maeder, A. & Meynet, G. 2012, A&A, 546, 105
- Osterbrock, D. F. & Ferland, G. F. 2006, *Astrophysics of Gaseous Nebulae and Active Galactic Nuclei* University Science Books
- Oudmaijer, R. D. 1998, A&A., 129, 541
- Oudmaijer, R. D., Groenewegen, M.A.T., Matthews, H.E., Blommaert, J.A.D., & Sahu, 1996, MNRAS., 280, 1062
- Riess, A. G., Fliri, J., & Valls-Gabaud, D. 2012, ApJ, 745, 156
- Scowcroft, V., Bersier, D., Mould, J. R., & Wood, P. R. 2009, MNRAS, 396, 1287
- Smartt, S. 2009, in Ann. Rev. Astron. & Astrophys., 47, 63
- Suh, K.-W. 1999, MNRAS, 304, 389
- Thompson, T.A., Prieto, J. L., Stanek, K. Z. et al. 2009, ApJ, 705, 1364
- Valeev, A. F., Sholukhova, O. N., & Fabrika, S. N. 2009, MNRAS, 396, L21
- Valeev, A. F., Sholukhova, O. N., & Fabrika, S. N. 2010a, Astrophysical Bull., 65, 149
- Valeev, A. F., Sholukhova, O. N., & Fabrika, S. N. 2010b, Astrophysical Bull., 65, 381

van Genderen, A. M., Sterken, C., & de Groot, M. 1997, A&A, 318, 81

van Genderen, A. M., de Groot, M., & Sterken, C. 1997, A&AS, 124, 517

van Genderen, A. M. & Sterken, C. 2002, A&A, 386, 926

Wright, E. L. Eisenhardt, P.R. M., Mainzer, A. K., et al. 2010, AJ, 140, 1868

Table 1. Journal of Observations

Target	UT Date	Spectrograph	Exp. Time	Grating & Tilt	Slit/Aperture(")	Seeing(")
M31-Blue	10 Oct. 2010	MMT/Hectospec	120m	600l, 4800Å	1.5	1.0
M31-Red	09 Oct. 2010	MMT/Hectospec	90m	600l, 6800Å	1.5	1.0
M33-Blue	03 Oct. 2010	MMT/Hectospec	120m	600l, 4800Å	1.5	0.4
M33-Red	03 Oct. 2010	MMT/Hectospec	90m	600l, 6800Å	1.5	0.4
M33-VarA	26 Sept. 2011	LBT/MODS1	21m	Dichroic	0.6	0.8 - 1.0
M33-B324	26 Sept. 2011	LBT/MODS1	15m	Dichroic	0.6	1.0 - 1.4
M33-N093351	28 Sept. 2011	LBT/MODS1	6m	Dichroic	0.6	0.5
M33C-4119	29 Sept. 2011	LBT/MODS1	12m	Dichroic	0.6	0.6
M31-004417.10	13 Oct. 2012	LBT/MODS1	12m	Dichroic	1.0	1.2
M31-004522.58	13 Oct. 2012	LBT/MODS1	18m	Dichroic	1.0	1.7
M33-N045901	14 Oct. 2012	LBT/MODS1	15m	Dichroic	1.0	0.9
M33-N125093	14 Oct. 2012	LBT/MODS1	15m	Dichroic	1.0	0.9
M33C-15731	14 Oct. 2012	LBT/MODS1	12m	Dichroic	1.0	0.7
M31-004425.18	17 Nov. 2012	LBT/MODS1	15m	Dichroic	1.0	1.3 - 1.6
M31-004444.52	17 Nov. 2012	LBT/MODS1	18m	Dichroic	1.0	1.2 - 1.5
M33C-7292	17 Nov. 2012	LBT/MODS1	12m	Dichroic	1.0	1.0 - 1.2
M31-004229.87	05 Jan. 2013	LBT/MODS1	23m	Dichroic	1.0	0.8

Table 2. The Warm Hypergiants in M31 and M33

Star Name	RA (2000)	Dec (2000)	Spec. Type	Other Id/Notes/References
M31				
M31-004322.50	J004322.50	+413940.9	late A - F0 I	
M31-004444.52	J004444.52	+412804.0	F0 Ia	
M31-004522.58	J004522.58	+415034.8	A2 Ia	
M33				
Var A	J013232.80	+303025.0	F8 Ia	Humphreys et al. (1987,2006)
N093351	J013352.42	+303909.6	F0 Ia	
B324	J013355.96	+304530.6	A8-F0 Ia	UIT 247
N125093	J013415.38	+302816.3	F0-F2 Ia	

Table 3. Multi-Wavelength Photometry (in magnitudes)

Star	U	B	V	R	I	J	H	K	3.6 $\mu\text{m}$ <sup>a</sup>	4.5 $\mu\text{m}$ <sup>a</sup>	5.8 $\mu\text{m}$ <sup>a</sup>	8 $\mu\text{m}$ <sup>a</sup>	3.4 $\mu\text{m}$ <sup>b</sup>	4.6 $\mu\text{m}$ <sup>b</sup>	12 $\mu\text{m}$ <sup>b</sup>	22 $\mu\text{m}$ <sup>b</sup>
M31-004322.50	20.7	21.2	20.3	19.9	19.2	...	...	...	14.9	14.6	14.4	13.5	15.7	15.5	12.3	9.1
M31-004444.52	19	19.1	18.1	17.3	16.6	15.8	15.2	14.4	12.6	11.8	11.2	10.2	12.6	11.7	8.6	6.5
M31-004522.58	17.9	18.6	18.5	18.2	18	17	16.3	15.4	15.4	15.6	13.7	11.9	14.2	13.3	10.8	8.5
M33-Var A <sup>c</sup>	20.2:	19.9	19.1	18.6	...	16.9	15.9	14.7	12.9	12.1	11.4	10.1	13.30	12.10	8.80	7.40
M33-N093351	16	16.4	16.2	16	15.7	15.7	15.3	14.7	13.0	12.6	...	10.3	...	...	...	...
M33-B324 <sup>d</sup>	14.9	15.3	14.9	15.2	15.0	13.7	13.4	13.3	12.7	12.5	...	...	12.50	12.15	8.30	5.90
M33-N125093	18.4	18.1	17.3	16.8	16.2	15.4	14.8	14.1	12.5	11.9	...	10.0	12.90	11.90	8.90	6.40

<sup>a</sup> *Spitzer*/IRAC

<sup>b</sup> WISE

<sup>c</sup>The photometry is from Humphreys et al. (2006). Recent CCD photometry obtained at the Barber Observatory, Univeristy of Illinois Springfield, in October and December 2012 suggests that Var A may have begun to brighten. Its current V magnitude is  $18.36 \pm 0.05$  measured relative to more than 40 comparison stars in the same field.

<sup>d</sup>B324 is in a very crowded region and groundbased visual photometry of B324 can be contaminated by nearby faint stars withn an arcsec or so of B324. For that reason we measured magnitudes from HST/WFPC2 F555W and F439W obtained November 30, 1998 which when converted to the standard V and B magnitudes give 15.12 and 15.56 respctively, slightly fainter than the groundbased photometry.

Table 4. Outflow Velocities ( $\text{km s}^{-1}$ )

Star	Double H $\alpha$	Double Ca II	P Cyg (H)	P Cyg (Ca II/[Ca II])	P Cyg (Fe II)
M31-004322.50	...	...	-326	-90	-200
M31-004444.52	...	...	-320	-254	-301
M31-004522.58	$\pm 100$	...	...	...	...
N093351	$\pm 120$	$\pm 70$	-92.5	...	...
B324	...	...	-143	-126	...
N125093	$\pm 220$	...	-160	...	...

Table 5. Circumstellar Densities based on [Ca II] and Ca II

Star	Photon ratio <sup>a</sup>	$n_e/(10^7 \text{ cm}^{-3})^b$
M31-004444.52	0.16	4.2
M31-004522.58	0.20	3.2
Var A	0.24	2.5
N093351	0.50	0.8
B324	0.37	1.4
N125093	0.36	1.4

<sup>a</sup>Ratio of multiplets,  $\Phi(\lambda 7300)/\Phi(\lambda 8600)$ .

<sup>b</sup>Assuming  $n_c = 8 \times 10^6 \text{ cm}^{-3}$  for collisional de-excitation of [Ca II]  $\lambda 7300$ .

Table 6. Mass Loss Estimates

Star	$W_\lambda(\text{H}\alpha)^a$ Å	Mass Loss Rate ( $M_\odot$ ) yr $^{-1}$ Thomson scattering	Mass Lost ( $M_\odot$ ) IR (SED)
M31-004322.50	96	$\sim 10^{-6}$ to $10^{-5}$	$0.09 \times 10^{-2}$
M31-004444.52	91	$10^{-5}$ to $10^{-4}$	$1.83 \times 10^{-2}$
M31-004522.58	171 (LBT)	...	$0.37 \times 10^{-2}$
Var A	43	$5 \times 10^{-4}$ , see text	2.40 to $0.8 \times 10^{-2b}$
N093351	29 (LBT)	...	$1.83 \times 10^{-2}$
B324	34 (LBT)	...	no dust
N125093	53	...	$2.40 \times 10^{-2}$

<sup>a</sup>The hydrogen emission lines in some of the hypergiants are contaminated with nebular emission. This is most obvious in the MMT spectra for B324 and N093351. We use their LBT spectra obtained with a narrower slit, see text and Figure 5 in the on-line edition.

<sup>b</sup>The mass lost from Var A is estimated from its flux in the  $9.8\mu\text{m}$  silicate feature at two different times during its high mass loss episode, 1986 and 2004, see text.

Table 7. Visual and Total Luminosities

Star	$A_v$ (colors) (mag)	$A_v$ (stars) (mag)	$M_v$ (mag)	$M_{Bol}$ (mag)
M31-004322.50	2.0	1.5	-6.1	-6.2
M31-004444.52	2.6	1.5	-8.9	-9.0
M31-004522.58	...	1.0	-6.9	-7.3
Var A <sup>a</sup>	...	...	...	-7.9
N093351	...	0.45	-8.8	-8.8
B324	0.8	0.9	-10.2	-10.1
N125093	1.6	0.9	-8.8	-8.9

<sup>a</sup>Var A is optically obscured by about 4 magnitudes of circumstellar dust. See text for a discussion of its luminosity.

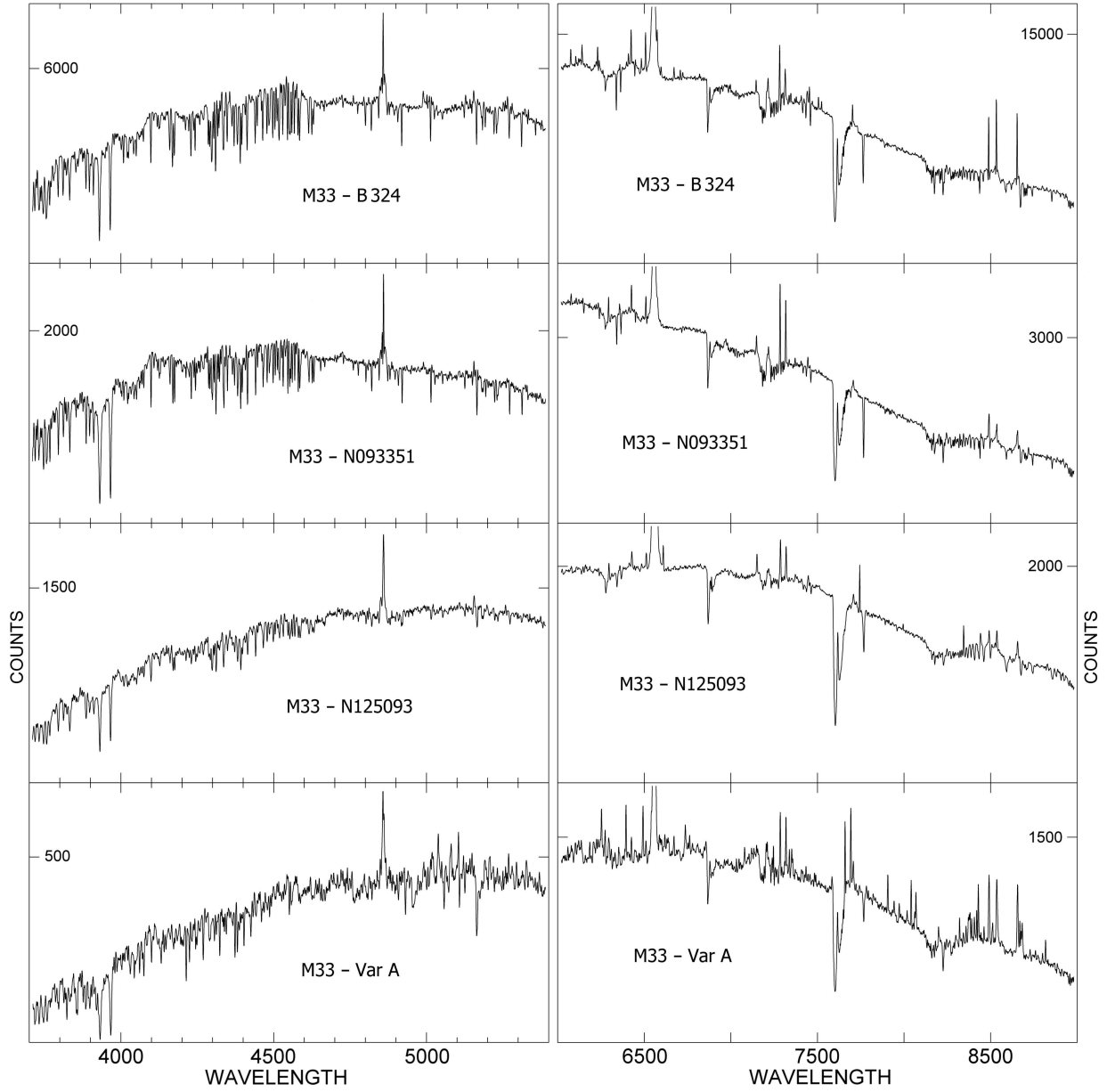


Fig. 1.— The blue spectra and red spectra of the warm hypergiants in M33. All spectra are from the LBT/MODS spectrograph.

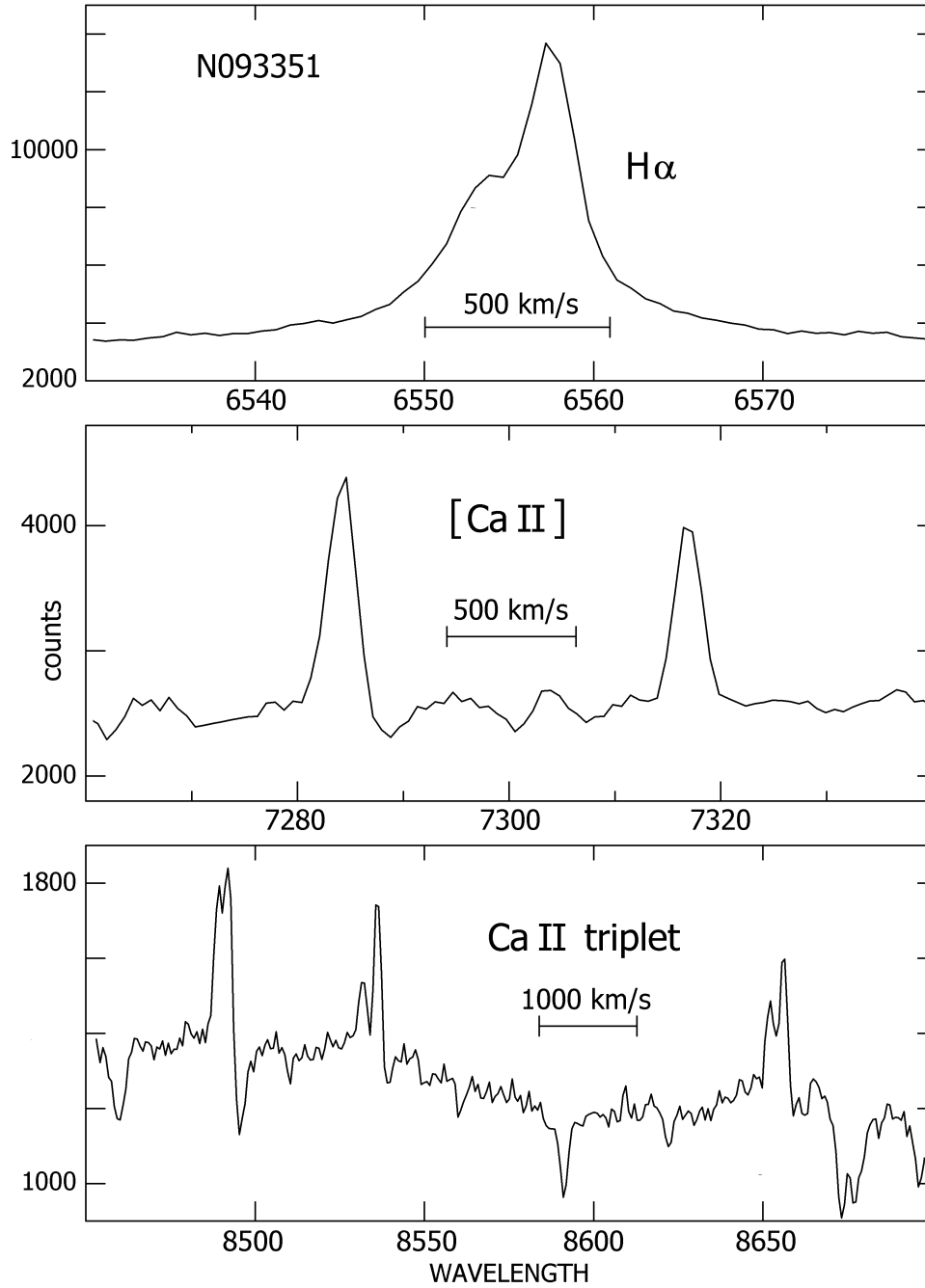


Fig. 2.— The H $\alpha$ , [Ca II] and Ca II triplet emission profiles in N093351. The double Ca II emission is not due to a blend with emission in the Paschen lines. Note that the Paschen line at  $\lambda 8598\text{\AA}$  is in absorption.

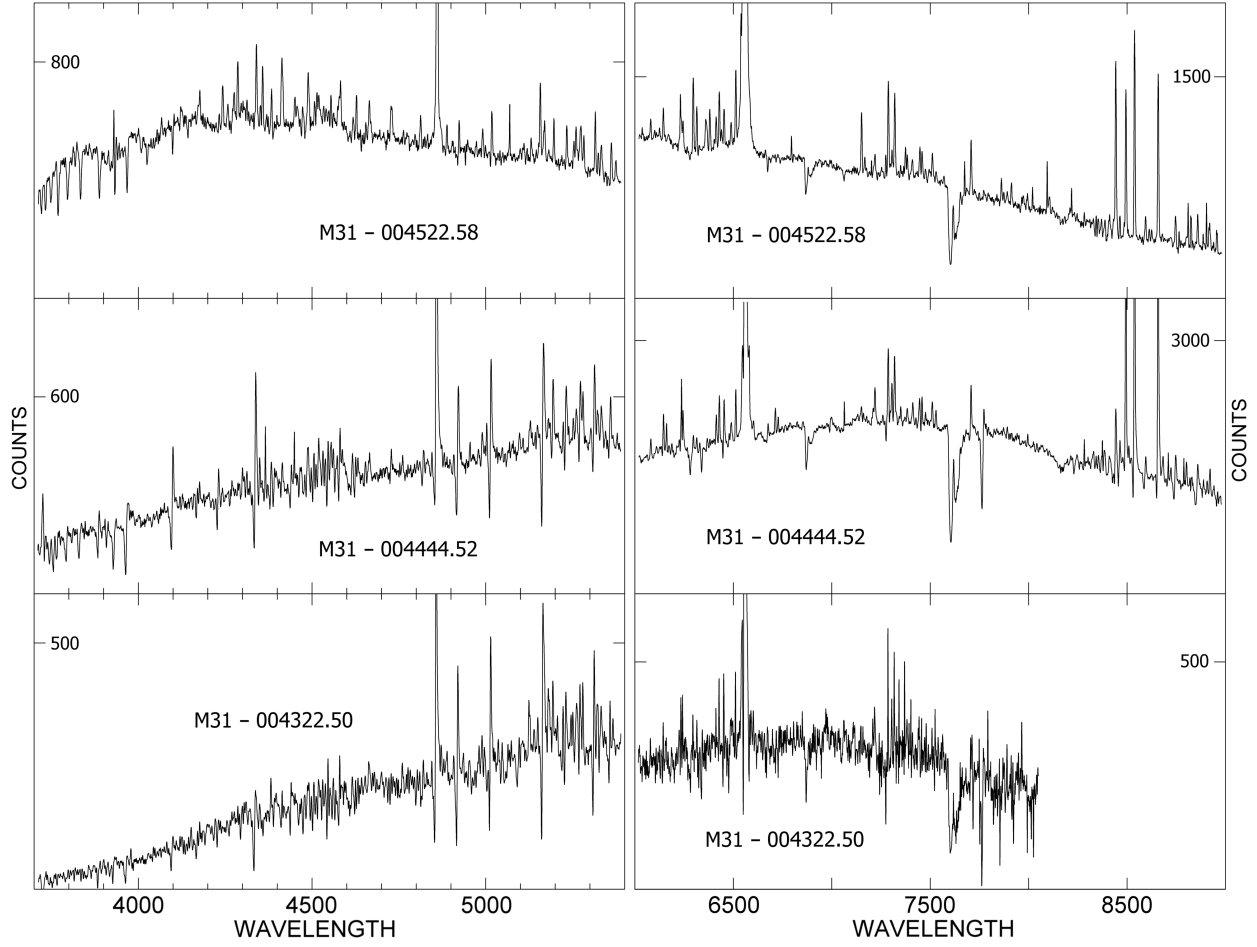


Fig. 3.— The blue spectra and red spectra of the warm hypergiants in M31. The spectra of M31-004322.50 are from the MMT/Hectospec and do not include the Ca II triplet in the far red.

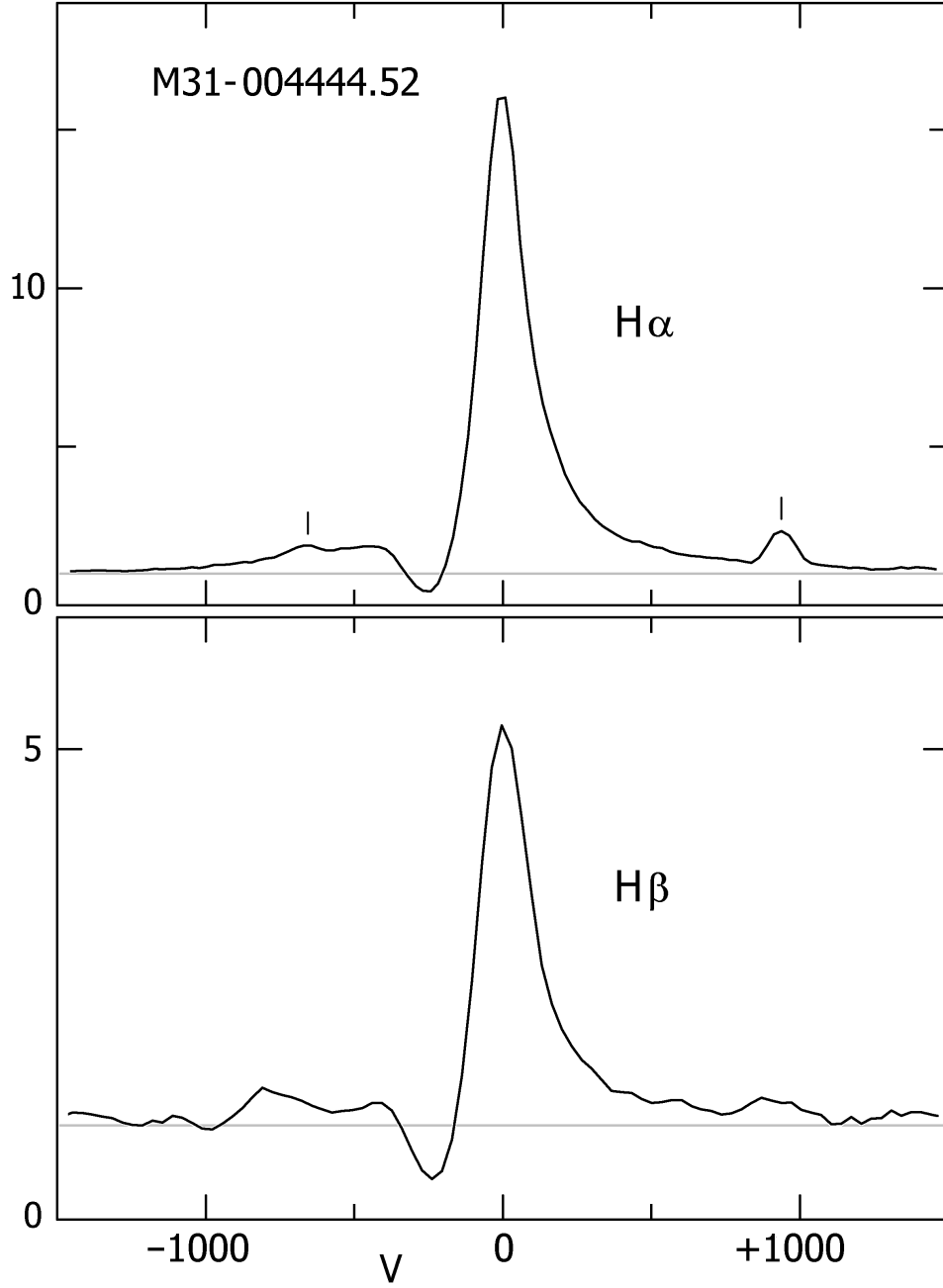


Fig. 4.— The asymmetric H $\alpha$  and H $\beta$  profiles for M31-004444.52. The tic marks identify the [N II] lines due to nebular emission.

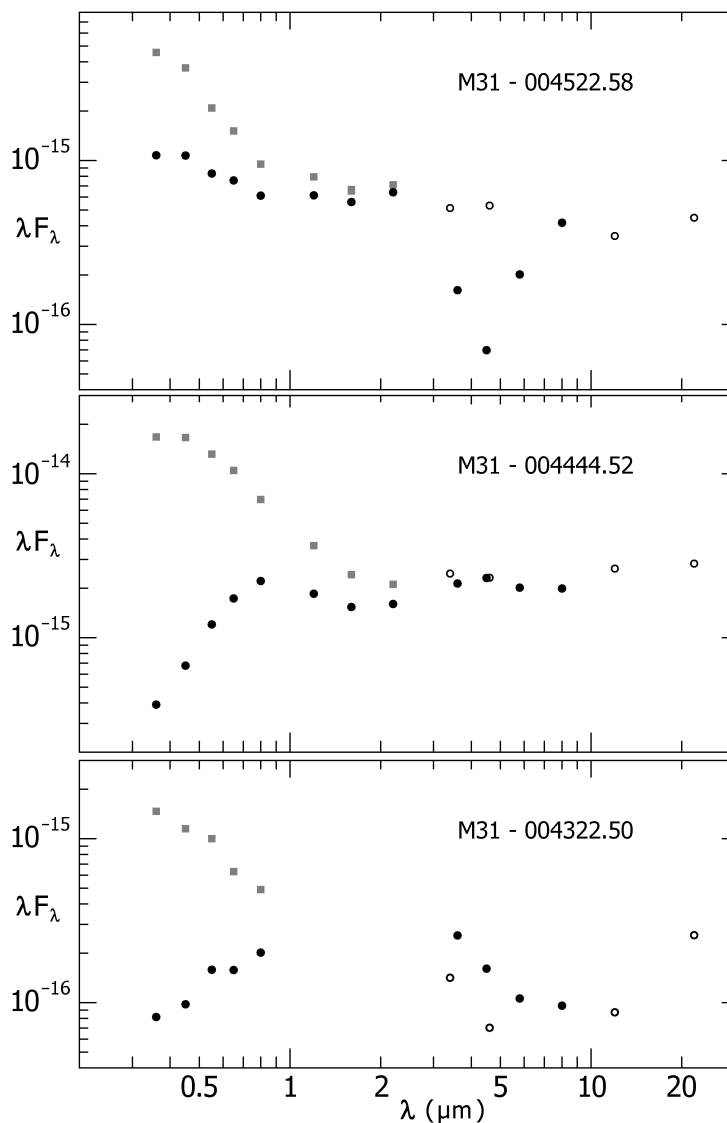


Fig. 11.— The SEDs for the three warm hypergiants in M31. The units are Watts/m<sup>2</sup> vs. wavelength in microns. The observations are plotted as filled circles with the WISE data as open circles, and the interstellar extinction corrected fluxes are shown as squares. The mid-infrared Spitzer and WISE photometry for M31-004522.58 are obviously discrepant. The prominent dip in the Spitzer data is the characteristic signature of an H II region; however its spectrum does not show any evidence for nebular emission and the longer wavelength WISE data does not show the rise in flux expected from an H II region. The upturn in the SED for M31-004322.50 at 20 $\mu\text{m}$  is most likely due to nebular emission.

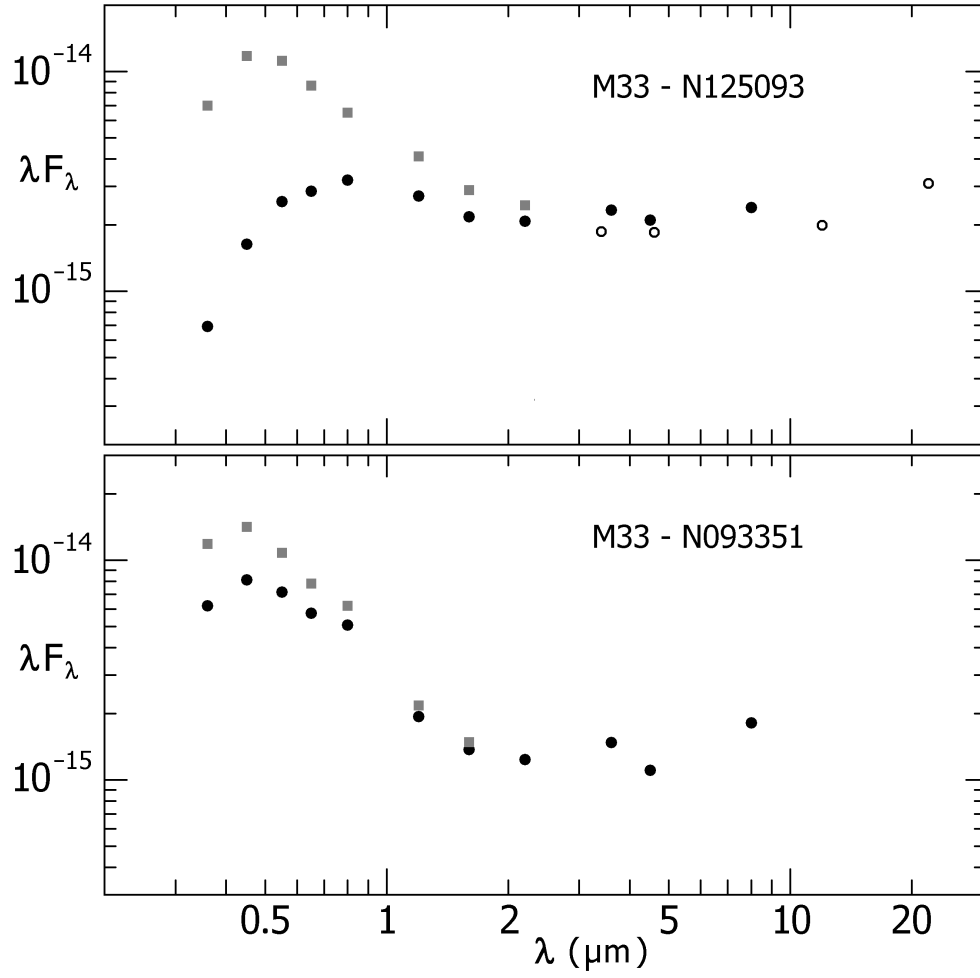


Fig. 12.— The SEDs for two warm hypergiants in M33. The units and symbols are the same as in Figure 11

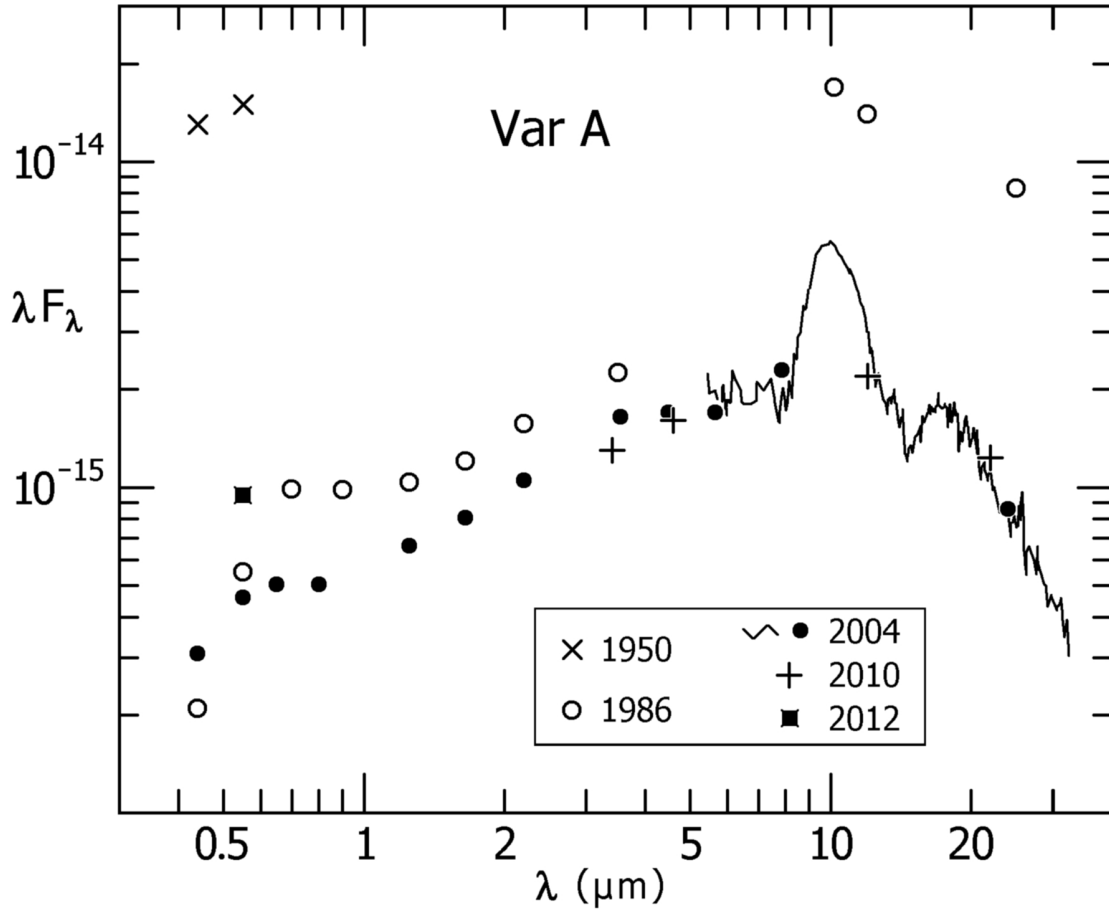


Fig. 13.— The SED for Var A reproduced from Humphreys et al. (2006) with addition of the WISE data (+’s) and the recent visual point plotted as a square (Table 3). The vertical scale is in Watts/m<sup>2</sup> for comparison with the other hypergiants.

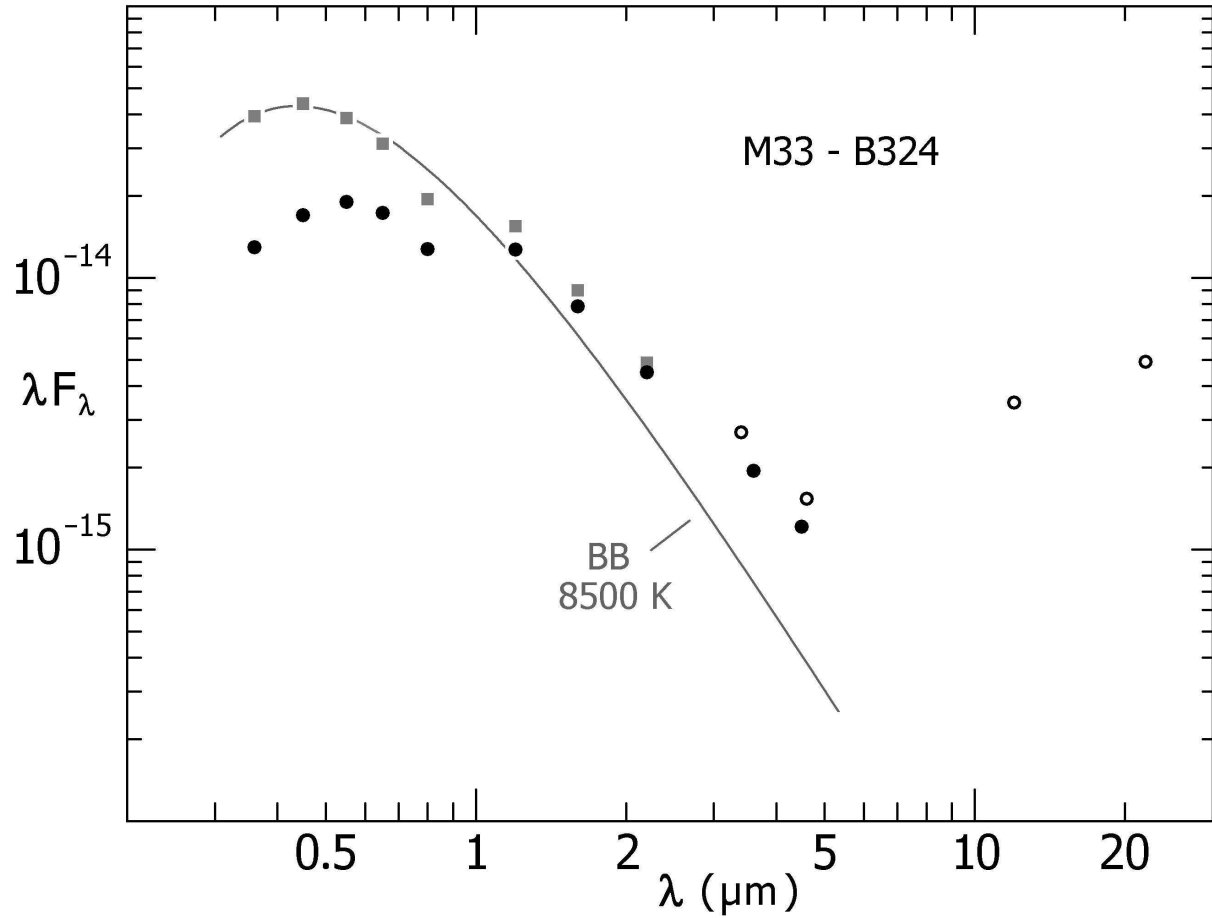


Fig. 14.— The SED for B324. The units and symbols are the same as in Figures 11 and 12. A 8500 K blackbody is shown fit through the extinction-corrected visual photometry, and illustrates that the near-IR excess is due to free-free emission. The increased flux longwards of  $10\mu\text{m}$  in the WISE data is most likely due to emission from the surrounding nebulosity.

